

GRAPHENE EDGE SPINS: SPINTRONICS AND MAGNETISM IN GRAPHENE NANOMESHES

T. Hashimoto¹, S. Kamikawa¹, Y. Yagi¹, J. Haruyama^{1*}, H. Yang², M. Chshiev²

¹Faculty of Science and Engineering, Aoyama Gakuin University, Kanagawa, Japan

²SPINTEC, CEA/CNRS/UJF-Grenoble 1/Grenoble-INP, 38054, Grenoble cedex 9, France

*J-haru@ee.aoyama.ac.jp

PACS 75.70.-i, 75.30.-m, 75.50.Dd, 75.75.-c

We have fabricated low-defect graphene nanomeshes (GNMs) by using a non-lithographic method and observed large-amplitude ferromagnetism even at room temperature, only when pore edges of the GNMs were hydrogen-terminated. The observed correlation between the inter-pore spacing and magnetism and also magnetic force microscope observations suggest that it is attributed to polarized electron spins localized at the zigzag-type atomic structured pore-edges. The magnetic moment per edge dangling bond ($\sim 0.3 \mu\text{B}$) is also in quantitative agreement with two theories. Moreover, a spin pumping effect is found for fields applied in parallel with the GNM planes in few-layer ferromagnetic GNMs, while a magnetoresistance (MR) hysteresis loop is observed under perpendicular fields. The present ferromagnetic GNMs must also realize rare-element free, invisible, flexible, and ultra-light (wearable) magnets and spintronic devices, which can overcome environmental and material-resource problems.

Keywords: Graphene, Edges, Polarized spins, Magnetism, Spintronics, Flat band.

1. Introduction

Graphenes, a mono-atomic carbon layer, has attracted considerable attention from many viewpoints. A variety of electronic structures, physical phenomena, and applications have already been reported. However, there is one issue, on which little data have been experimentally reported. That is edge-based phenomena. There are two different kinds of edge atomic structures for graphenes. One is the so-called arm chair, while the other is zigzag. It is theoretically well-known that zigzag edges can produce a flat energy band, where electrons have infinite effective mass and, hence, localize, resulting in extremely high electronic density of states (EDOS); the so-called edge states. Due to the edge states, spin interaction is significantly induced. Then, electron spin polarization (e.g., (anti)ferromagnetism) can appear spontaneously [1–7, 10–22, 28–31].

In the case of a graphene nanoribbon (GNR), which is an one-dimensional strip line of graphene with edges on both longitudinal sides, the edge-based spin configuration is very complicated and thus, interesting [1–7]. Assuming perfect edges for GNRs without any defects allows the electron spins localized at zigzag edges [1, 10] to be stabilized toward polarization (i.e., (anti)ferromagnetism) due to the exchange interaction between the two edges, which produces a maximum spin ordering in these orbitals as well as those in graphene nanomeshes (GNMs) with hexagonal nanopore arrays (Fig.1) [13, 29], and in graphene nanoflakes [14]. This is similar to the case of Hund's rule for atoms. Moreover, the spin configuration depends on different kinds of atoms (e.g., hydrogen (H) and oxygen (O)), which terminate edge carbon dangling bonds [3, 31].

Conversely, assuming the presence of defects in the ensemble of carbon atoms (e.g. graphene flakes) yields a net magnetism, which is interpreted by Lieb's theorem. It predicts the emergence of ferromagnetism by an increase in the difference between the number of removed A

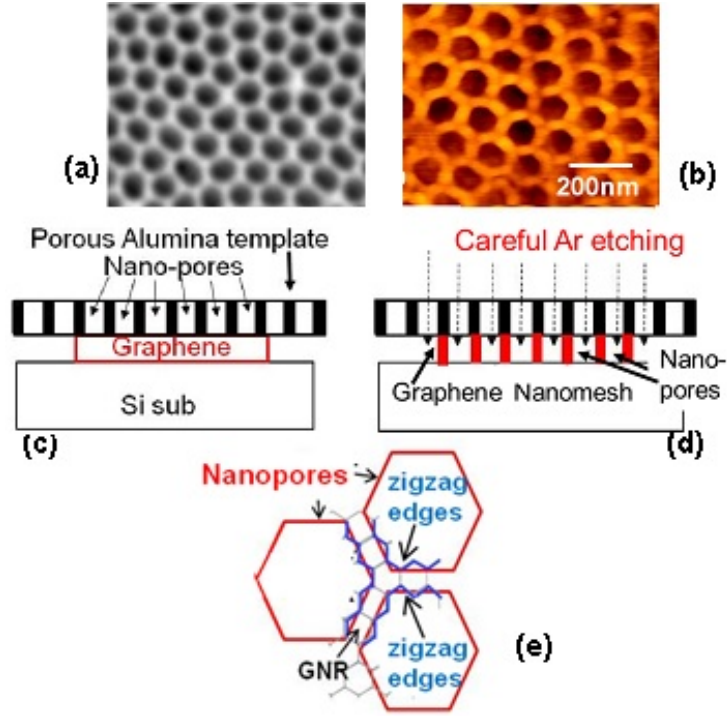


FIG. 1. (a) SEM top view of an NPAT, which shows honeycomb-like array of hexagonal nano-pores. (b) AFM image of a GNM formed by using (a) as an etching mask, which proves hexagonal shape of pores with mean diameter $\phi \sim 80$ nm and mean inter-pore distance $W \sim 20$ nm. (c)(d) Schematic cross sectional views of fabrication process of a GNM. (c) NPAT is located on graphene as an etching mask. (d) The graphene is carefully etched by Ar gas, resulting in a GNM. (e) Schematic view of a GNM with the zigzag-type pore-edge. Narrow regions sandwiched by two pores with width (W) correspond to GNRs. Actual structure includes a larger number of hexagonal carbon unit cells per inter-pore region with ~ 40 nm length and $W \sim 20$ nm. This GNM structure brings at least three large advantages

and B sites (Δ_{AB}) of the graphene bipartite lattice at zigzag edges [14,29,31]. The magnitude of the ferromagnetism increases with increasing values of Δ_{AB} .

Moreover, many theoretical works have predicted spin-based phenomena realizable using graphene edges. For instance, a spin-filtering effect predicted that GNRs with antiferromagnetic spin alignment on two edges can transport only electron spins with the same moment, which can be controlled by applying electric fields [22]. Realization of (quantum) spin Hall effect (SHE) as topological insulator (TI) was also theoretically predicted by resolving double degeneration of edge spin bands (e.g., by introducing spin orbit interaction (SOI)) and controlling two spins with opposite moments existing in two different bands by applying electric fields [25–27]. Indeed, one group reported on the observation of SHE in dihydrogenated graphenes. Using a specified resist (MSQ) and irradiating electron beam with changing the amount of dose allowed dihydrogenation of the graphenes including edges. This resulted in the appearance of sp^3 hybridized orbitals and, hence, introduction of strong SOI and SHE. These are strongly expected to make possible novel spintronic devices.

No works, however, have reported experimental observation of magnetism and spin-based phenomena arising from graphene zigzag edges, although the observation of graphene

edge-atomic structures has been carried out in some systems (e.g., in overlapped graphenes with Joule heating [15], GNRs [17–19], and GNMs with pore edges [20,21]). This is because edge-related phenomena are easily destroyed by disorder (damage, defects) introduced during the fabrication process (e.g., by lithographic methods). We have, therefore, developed two non-lithographic fabrication methods for graphene edges; i.e., (1) GNRs derived from unzipping of carbon nanotubes combined with air blow and three-step annealing [17] and (2) GNMs fabricated using a nanoporous alumina template (NPAT) [33]. In the present work, magnetism and spin-related phenomena are reported for GNMs made using the latter process.

2. Experimental results and discussion

2.1. Ferromagnetism arising from pore edges

(a) Sample fabrication

Low-defect GNMs with honeycomb-like arrays of hexagonal nanopores (Figs. 1(b) and 1(e)) were fabricated on a large ensemble of mechanically exfoliated graphenes (or CVD-synthesized graphenes on a SiC substrate) by using NPAT (Fig. 1(a)) [23] as an etching mask (Fig. 1(c)), following our previous method [33]. The NPAT, which consists of a honeycomb-like array of hexagonal-shaped nanopores, was fabricated by the anodic oxidation of a pure aluminum (Al) substrate (Al = 99.99%) using electrochemical methods with a carbon cathode [23]. Due to self-organization, a NPAT provides structure parameters (e.g., pore diameter ϕ and interpore space w) with exceptionally high regularity and high reproducibility. After the formation, the NPAT with an area of 1 cm² was detached from the Al substrate by alternating the polarity of the two electrodes. The detached NPATs were then placed onto the graphenes on Si(SiO₂) substrate as etching masks.

The thin-multilayer (< 10 layers) and monolayer graphene samples which were used as the base for formation of GNMs were extracted from bulk Kish graphite (Toshiba Ceramics) onto degenerately doped Si wafers with a 250-nm-thick SiO₂ surface layer by means of mechanical exfoliation. Interference-induced color shifts in an optical microscope (3D-CCD), Raman spectroscopy, and cross-correlation with an AFM profile allowed us to identify the number of deposited graphene layers of all graphene flakes, which ranged from 1 to ~10.

Using the NPAT as a mask, the assembled graphenes were etched by a carefully optimized low-power Ar gas (e.g., 200–600 V for 10–40 min) to avoid damage. We carried out the low-power etching step by step. After each 10 minute etching, we performed a FESEM (or AFM) measurement and checked for the formation of nanopores on the Si-substrate under the NPAT mask. Until the formation of nanopores on the Si-substrate was confirmed, we repeated the low-power etching. This is a very important process which avoids damaging the pore edges. The boundaries of nanopores are not aligned along the hexagonal carbon lattice of graphene in this process. Consequently, naomesh of the NPAT was transferred to graphene. After formation of the GNM, the NPAT mask was entirely dissolved by a H₃PO₄ solution or detached mechanically from the GNMs in some cases. Either method left no contamination remaining from the NPAT mask. Then, all multi-layer GNM flakes (i.e., except for monolayer GNMs), which existed under the NPAT, were entirely removed by the mechanical method (i.e, by plastic tweezers) one by one to measure the magnetization of only monolayer GNMs. After removing, the absence of the multi-layer GNM flakes was reconfirmed following the above-mentioned method.

All GNMs fabricated through these processes (including Figs. 2(c) and 2(f) sample) were annealed at 800 °C under high vacuum (10⁻⁶ Torr) for 0.5–3 days with constant gas pumping and, then, under hydrogen gas by a field-emission-type radical CVD system under greater than

1MPa pressure for at least for 3 hours for all the measurements. The first annealing is for deoxygenation of the pore edges and recovering all damages and defects, while the second annealing is for termination of the carbon atoms at the pore edges by hydrogen atoms.

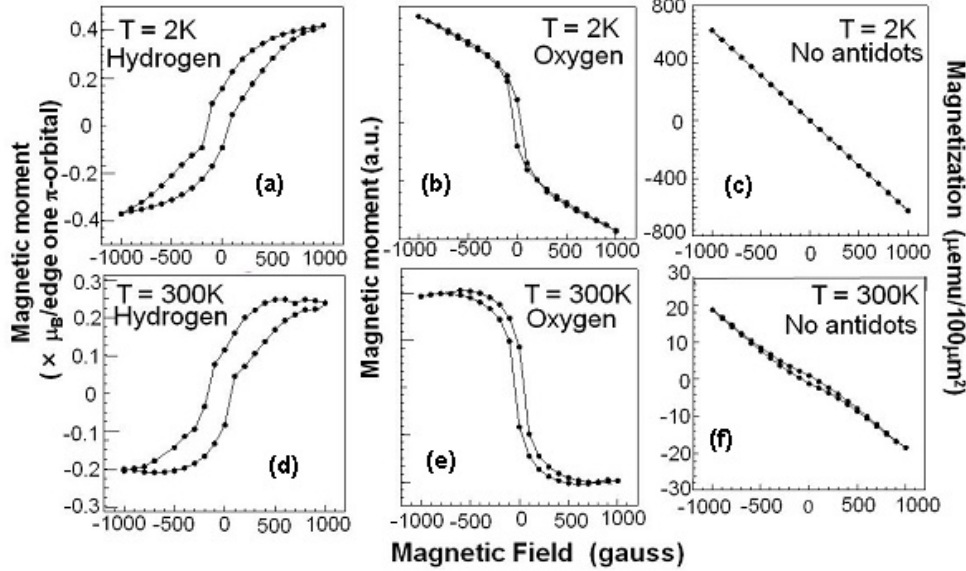


FIG. 2. Magnetization of monolayer GNMs with $\phi \sim 80$ nm and $W \sim 20$ nm for (a)(d) hydrogen-terminated edges; (b)(e) oxygen-terminated edges; and (c)(f) bulk graphene without pore arrays. DC magnetization was measured by a superconducting quantum interference device (SQUID; Quantum Design). Magnetic fields were applied perpendicular to GNMs. The vertical axes in panels (a) and (d) denote magnetic moment per localized-edge orbital, assuming mono-hydrogenation of individual edge carbon atoms

The observation of the features shown in Figs. 2(b) and 2(e) were made after the observation of the feature in Fig. 2(a), and subsequent annealing at 800 °C under high vacuum (10^{-6} Torr) for 3 days with constant gas pumping for dehydrogenation of the edges and, then, under an oxygen atmosphere for 1 hour for oxidization of the pore edges. SQUID measurements were carried out immediately after annealing.

Consequently, a large ensemble of monolayer GNMs with a total area $\sim 4 \times 1$ cm² was prepared for magnetization measurements (Fig. 2) (i.e., one sample consists of at least 4 substrates with monolayer GNMs. The total area does not include the area of the nano-pores. The total number of measured samples was 11). In order to confirm the lack of contribution from NPATs and Si-substrates, the magnetization of the Si-substrates assembled with only NPATs (i.e., without GNMs) was measured as well as the NPATs for Figs. 2(c) and 2(f) (Si-sub + bulk graphenes) and the absence of ferromagnetism was confirmed.

This method offers the following three significant advantages. (1) It gives less damage and defects to the GNMs because of the non-lithographic method. (2) Moreover, the honeycomb-like array of hexagonal nanopores can result in the formation of a large ensemble of GNRs and pore edges with sufficient lengths (e.g., 40 nm in the present case), because the regions between two pores can be GNRs and the presence of six boundaries of hexagonal pore among the neighboring six pores produces six GNR (Fig. 1(e)). In the actual GNM, it is speculated that a mixture of zigzag and armchair edges may exist in one GNR (one pore edge), as confirmed by the STM observation [9]. Even in that case, a large number of GNRs in the present GNMs can

yield a large area of assembled zigzag-edge GNRs. This is extremely effective to detect small magnetic and electric signals arising from pore edges. (3) From a topological reason, when the atomic structure of one pore boundary is aligned with the hexagonal carbon lattice of graphenes (e.g., to zigzag), the other five pore boundaries can have the same edge atomic structure (e.g. zigzag).

In the present experiment, the pore-edge atomic structures could not be intentionally controlled to zigzag type unlike Ref. [20]. However, in Ref. [33], we indirectly proved the presence of zigzag atomic structure at the pore edges by observation of the small ratios of D/G peak heights (< 0.2) in Raman spectroscopy, which were realized by reconstruction of edge atomic structure to a zigzag type by high-temperature annealing, in comparison with previous reports [20, 30]. Indeed, the presence of polarized spins in such H-terminated GNMs was confirmed in inter-pore regions and also at some pore edges by observations using magnetic force microscopy [33]. Moreover, the observed anomalous magnetoresistance (MR) oscillation turned out to be due to the presence of localized electrons at the pore edges in the H-terminated zigzag-type GNMs with ~ 10 layers [33].

(b) Magnetism due to H-terminated pore edges

The magnetization curve measured for the H-terminated monolayer GNM, which showed the low D/G peak ratio values (< 0.2), is shown in Fig. 2(a). A ferromagnetic-hysteresis loop with large amplitude is clearly observed. In addition to this sample, three other samples with low D/G peak heights in Raman spectroscopy exhibited similar ferromagnetism. In contrast, O-terminated GNMs exhibited a diamagnetism-like weak hysteresis loop (Fig. 2(b)). This is consistent with Ref. [6], which reported that the formation of a spin-paired C–O chemical bond drastically reduces the local atomic magnetic moment of carbon at the zigzag edge of GNRs and suppresses the emergence of ferromagnetism. Reference [6] reported that the formation of a spin-paired C=O chemical bond drastically reduces the local atomic magnetic moment of carbon at the zigzag edge of GNRs and suppresses the emergence of ferromagnetism. The disappearance of ferromagnetism in Figs. 2(b) and 2(e) is qualitatively consistent with this theory.

Bulk graphenes without any pores and those assembled with NPATs show few such features, even after H_2 annealing (Figs. 2(c) and 2(f)), implying no contribution of parasitic factors (e.g., defects, impurities) from bulk graphenes. Moreover, presence of less damage or impurities was reconfirmed in most of the bulk-graphene regions, because mechanically exfoliated bulk graphenes showed extremely low D/G peak heights ($\ll 0.1$) and high 2D peak intensity in Raman spectroscopy. These results strongly suggest that the observed ferromagnetism is associated with polarized spins localized at the H-terminated zigzag-pore edges. The ferromagnetism observed at 2 K appears even at room temperature with a larger magnitude for the hysteresis loops (Fig. 2(d)). In Figs. 2(b) and 2(e), even the diamagnetism of graphene has mostly disappeared. One of the reasons is attributed to the formation of a nanopore array, because such an array drastically reduces the bulk graphene area available for the presence of loop currents which produce diamagnetism at the currently applied magnetic-field levels (i.e., corresponding to only GNRs with $W \sim 20$ nm between nanopores; Fig. 1(e)). The radius of the cyclotron motion for electrons is given by $R_c = (\pi n_s)^{1/2} (h/2\pi) / eB$. By observing the magnetoresistance (i.e., commensurability peak), we calculate n_s to be $\sim (4 \times 10^{11}) \text{ cm}^{-2}$ in the present GNMs. Based on this n_s value, R_c is calculated to be as large as ~ 400 nm, even for the largest applied magnetic field of 1000 gauss in Fig. 2. Indeed, this R_c value is 20 times larger than $W \sim 20$ nm between the present nanopores, and it prohibits the emergence of loop currents for the formation of diamagnetism.

Figure 3 shows the correlation between the inter-pore spacing (corresponding to the width of the GNR, W ; Fig.1(e)) and the magnetization. The magnitude of the hysteresis loop was found to decrease with increasing W . In particular, the residual magnetization is inversely proportional to the W value (inset of Fig. 3(c)). This result is qualitatively consistent with theories for the GNR model, according to which, the edge spin stability and ordering of a zigzag-edge GNR are determined by the exchange interaction between the two edges leading to vanishing of ferromagnetic edge spin ordering with increased W [2,5].

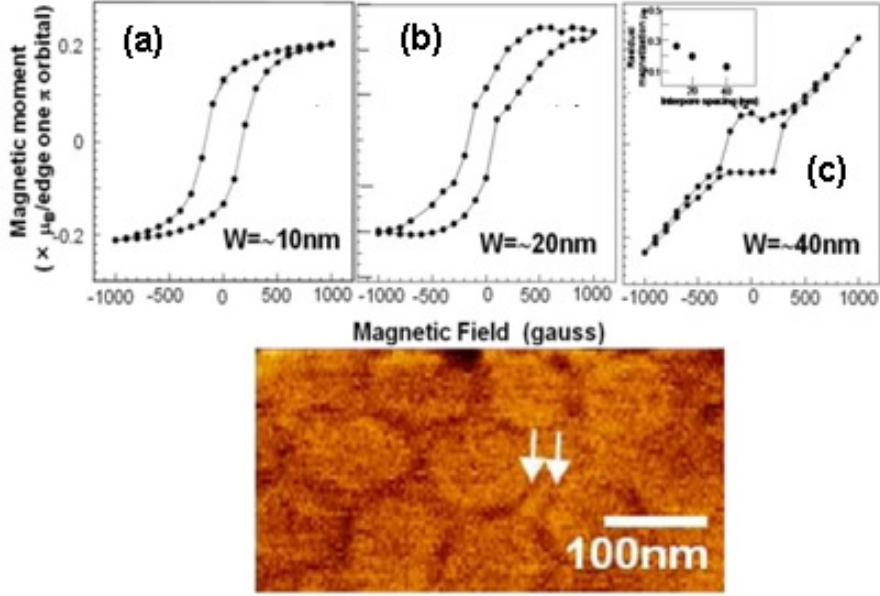


FIG. 3. (a)–(c) Correlation of the magnetization with the mean inter-pore spacing W of monolayer GNMs at $T = 300$ K. Mean pore diameter ($\phi \sim 80$ nm) was kept through all samples. For Figs. 3 (a)–(c), difference in magnetic moment between upper and lower curves of hysteresis loop at $H = 0$ (residual magnetization $B_r \times 2$) is $\sim 0.28 \mu_B$, $\sim 0.2 \mu_B$, $\sim 0.12 \mu_B$ and the loop width at zero magnetic moment (coercivity $H_c \times 2$) is ~ 400 gauss, ~ 260 gauss, ~ 500 gauss, respectively. Inset of (c); B_r at 300 K as a function of W . (d) Magnetic force microscope image of a ferromagnetic GNM. CoPtCr-coated Si-probe was used for measurement with a tapping mode. Darker color means higher densities of polarized spins. In particular, the parts indicated by two arrows evidently show presence of pore-edge localized spins

Such a correlation cannot be understood by ferromagnetism originating from the defects located only at the pore edges or in the bulk graphene between pores. In the former case, the ferromagnetism amplitude should be mostly independent of W , because defects are located only at pore edges. In the latter case, the ferromagnetism amplitude should increase with an increase of W , because the defect density increases. Consequently, we conclude that the observed ferromagnetism is not due to parasitic origins (e.g., defects, impurities) but should be truly attributed to H-terminated zigzag pore edges.

This is also consistent with magnetic force microscope (MFM) observations (Fig. 3(d)). Although the space resolution is poor, we can actually confirm the presence of high densities of polarized spins at the inter-pore regions and also some pore edges under slight magnetic fields. To date, approximately 50% of the samples, which include samples showing the low D/G peak heights, have shown ferromagnetism.

As mentioned above, we could not intentionally form zigzag-type pore-edge atomic structure. Refs. [15] and [16], however, suggested that zigzag edges are the most stable chemically and that arm chair-based edges are reconstructed to zigzag after STM Joule heating for long edges of overlapped graphenes [15] and electron beam (EB) irradiation for pore edges [16].

Ref. [30] reported that edge chirality can be distinguished by the observation that the $I(D)$ for graphene edges were stronger (weaker) at the armchair (zigzag) edges. This is because the double resonance process, which induces the D peak, can only be fulfilled at an armchair edge, when the one-dimensional character of the edge is considered. Indeed, Ref. [30] exhibited $I(D)/I(G)$ value < 0.1 for observation of zigzag edge of graphene flakes by using angle-dependent Raman spectroscopy with a polarized laser beam. This is qualitatively consistent with Fig. 1(e).

The low $I(D)/I(G)$ values are also qualitatively consistent with those reported for GNPs in Ref. [20], whose hexagonal-pore boundaries are intentionally aligned along the carbon hexagonal lattice by specified method, resulting in the formation of pure zigzag pore edges.

There are three different edge structures: zigzag, armchair, and a mixture of the two. Because the possibility of the formation of each structure is basically equal ($\sim 33\%$), the value of 50% for formation of a zigzag edge (samples 1–4) indicates that almost half of the edges for the case of the mixtures (i.e., $\sim 33\%/2 = \sim 17\%$), which are close to the behavior of a zigzag edge, can be reconverted to a zigzag edge by annealing (i.e., $\sim 33\% + \sim 17\% = \sim 50\%$). The remaining 50% of the samples will have armchair edges or large-volume defects.

The stability may be simply understood by the difference in the number of carbon atoms bonded to two neighboring carbon atoms (dangling bonds) for zigzag edge (i.e., one such atom) and arm chair edges (two such atoms) [16]. After removal of such atoms, the arm chair edge requires twice as much energy as the zigzag in order to repair the removed atoms and, thus, becomes unstable. In our system, we carried out high -temperature annealing for narrow ($W \sim 20$ nm) GNRs (i.e., narrow inter-pore spacing). This might bring the energy similar to those in Refs. [15,16] and cause the reconversion of edge atomic structures to zigzag.

However, this is strongly case-dependent. Edge reconstruction occurs under some conditions; e.g., electron beam (EB) irradiation during HRTEM observation (Ref. [16]), Joule heating by a STM probe (Ref. [15]), and high temperature annealing. Thus, the exact values of activation energy for cutting and reconstructing edge C-C bonds should be experimentally investigated and be determined as universal values in the future.

Currently, refs. [15] and [16] argue that the zigzag edge is the most stable and arm chair-based edges are reconverted to zigzag ones after EB irradiation for pore edges and STM Joule heating for long edges of overlapped graphenes, while “PRL 101, 115502” and “PRB 80, 073401” interestingly argues that 5–7 zigzag edge is stable after EB irradiation. These results may look controversial.

However, to the best of our knowledge and experience, 5–7 edge structures have been merely observed and reported to date, because they consist of peculiar polygons except for hexagon. Indeed, the “PRB 80, 073401” exhibited only very small parts of the edges. Thus, we don’t think that the 5–7 edge can stably exist within a long range along long edges like our hexagonal nanopore with a 40 nm length for one boundary. Moreover, 5–7 edge can be one of disordered edge structures and, hence, large $I(D)/I(G)$ ratios should be observed in Raman spectroscopy. This is not consistent with our results. Therefore, we concur with the argument put forth in refs. [15] and [16].

The observation of edge atomic structures is indispensable for present experiments. However, it is extremely difficult to do this at this time, because for HRTEM observation,

GNMs cannot be fabricated on a TEM grid, and for STM observation, the GNMs do not have a large enough conductivity for such measurements. The GNMs formed on Cu substrates may solve this problem for STM observations, because such a substrate provides a high conductivity, although the atomic edge structures may be affected by the Cu substrate.

(c) *Theoretical discussion of edge magnetization values*

Here, employing the GNR model, which assumes pure zigzag pore edges (i.e., without any defects) at all regions, allows one to estimate the magnetic moment of edge carbon atoms that contribute to the ferromagnetism observed in Fig. 2. Assuming that only edge dangling bonds have localized spin moments, the magnetic moment per edge dangling bond prior to H termination is estimated to be $(1.2 \times 10^{-23}) / (\mu_B = 9.3 \times 10^{-24}) \sim 1.3\mu_B$, where μ_B is the Bohr magneton, as follows.

(1) The total area of assembled bulk graphenes used for the pore array formation is $\sim 4 \text{ cm}^2$. (2) The area of one hexagonal unit cell with a pore is $S = 6(3^{-1/2}/2)(a/2)^2 \sim 4300 \text{ nm}^2$, where $a = [80 \text{ nm (pore diameter)} + 20 \text{ nm (interpore spacing)}]$. (3) Thus, the total number of pores is $(4 \text{ cm}^2)/(4300 \text{ nm}^2) \sim 1011 [(1)/(2)]$. (4) The total number of dangling bonds per hexagonal pore is $(40 \text{ nm})/(0.142 \text{ nm} \times 3^{1/2}) \times 6 = 166 \times 6 \sim 1000$. (5) The total number of edge dangling bonds of the GNM used for the SQUID measurement is $1014 [(3) \times (4)]$.

Therefore, using (5), the saturation magnetization per edge dangling bond is estimated to be $1.2 \times 10^{-6} \text{ (emu)} \times 10^{-3}/10^{14} = 1.2 \times 10^{-23} \text{ (J/T)}$. Thus, the magnetic moment per edge dangling bond is estimated to be $(1.2 \times 10^{-23})/(\mu_B = 9.3 \times 10^{-24}) \sim 1.3 \mu_B$. This value is very large compared with previous theoretical predictions. Conventionally, GNRs with no H-termination of dangling bonds should show antiferromagnetism, theoretically. However, in the above estimation, the observed total magnetization was divided by estimated number of edge dangling bonds in the GNM, neglecting this theory. This led to the problem.

Next, after H annealing at high temperature, edge dangling bonds of a GNR are terminated by H atoms [3, 5–7, 9]. The following three types of H terminations are theoretically possible. (1) All edge dangling bonds are each terminated by one H atom on both -side zigzag edge. This provides a flat band for $2\pi/3 \leq k \leq \pi$ in the Brillouin zone. Electrons are well localized at the edges. (2) All the edge dangling bonds of one side are each terminated by two H atoms (so that the edge carbon atom becomes tetrahedrally coordinated; a bearded edge), while the opposite-side dangling bonds are terminated by a single H atom. The GNR provides a flat band for $0 \leq k \leq \pi$, resulting in a completely localized “on-bonding state” around the Fermi level (E_F). This leads to the spin polarization of all carbon atoms. (3) The double H atom termination of the zigzag-edge carbon atoms on both sides of a GNR provides a flat band for $0 \leq k \leq 2\pi/3$ and creates a modified zigzag edge.

The type of edge H-termination could not be observed in the present experiment. However, our case should correspond to case (1) for the following reason; the mono-H termination of the edge dangling bond decreases its magnetic moment to one μ_B . The magnetic moment of one localized-edge π orbital is, therefore, estimated to be as large as $(\sim 1.3\mu_B - 1 \mu_B) = \sim 0.3 \mu_B$. This is in fairly good agreement with the theoretical contribution of the π -orbital state to the edge magnetic moment of $\sim 0.3 \mu_B$ in a zigzag-edged GNR within the ferromagnetically ordered spin configuration [5].

We have estimated the edge magnetization based on a GNR model with zigzag edges, assuming the presence of perfect zigzag-pore edges at all parts of our GNMs. In contrast, even a small defect may still be present in actual pore edges. In order to elucidate the influence of such residual small-volume edge disorder on GNM magnetism, we performed systematic first-principles calculations of magnetic properties of quasi-GNR structures (Fig. 4(a), corresponding

to the inter-pore region) based on Lieb's theorem [29], which assumes slight disorder at the upper edge. Interestingly, the ground state of quasi-GNR structure turned out to be ferromagnetic in Fig. 4(b). The calculated net magnetic moment follows Lieb's theorem with local moments up to $0.2 \mu_B/\text{edge atom}$ and depends on magnitude of the assumed edge disorder. These values agree fairly well with the value estimated from the GNR model. In order to determine which models are more relevant to the actual structures, observation of pore edge atomic structures is indispensable.

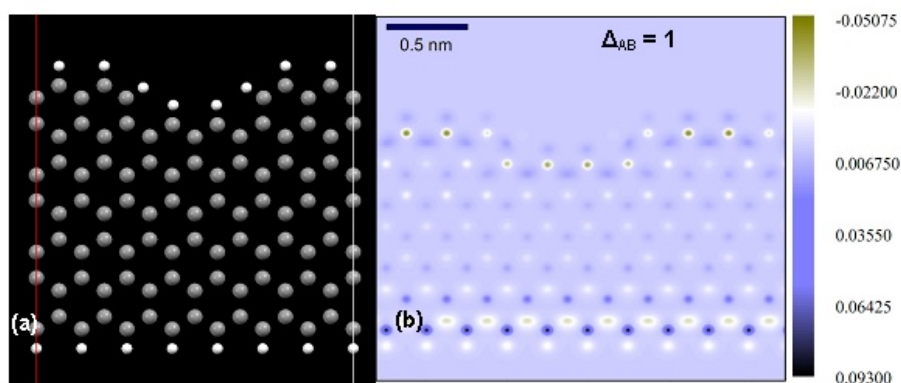


FIG. 4. Model and calculation result for net magnetism (Lieb's theorem) (a) Structure of hydrogen-passivated quasi-GNR, which employs slight curvature (disorder) with $\Delta_{AB} = 1$ (the difference between the number of removed A and B sites of the graphene sublattices at zigzag edges) on the upper edge, used for first-principles calculations based on Lieb's theorem. The dark and white atoms are carbon and hydrogen, respectively. (b) Calculated spin-density distribution of quasi-GNR for (a), which gives the edge magnetic moment of $0.2 \mu_B$ to the lower edge

2.2. Novel spin-phenomena in few-layer ferromagnetic GNMs

Although we have reported spin polarization at the pore edges of monolayer GNMs in the present study, the GNMs didn't show clear electronic features, because lithography was used for electrode formation on the monolayer GNM. This method introduced contamination and disorder to the pore edges. The resistivity of the GNMs was also very high.

In contrast, as mentioned above, we reported periodic MR oscillations arising from electrons localized at H-terminal pore edges in weak-ferromagnetic GNMs with ~ 10 layers, when magnetic fields were applied perpendicularly to the GNMs layers [33]. The observed oscillation period proved that the electron orbit localizing at the pore edges produced the oscillation with a period, which is shorter than those caused by cyclotron-motion electrons due to applied fields. This result suggested that contamination and disorder exist only around the topmost surface or the sub-surface layers, while lower layers (e.g., the fifth layer) should have mostly no such influence. Thus, also in the present measurements, we measured MR behaviors of H-terminated GNMs with ~ 5 layers. Although the magnitude of spin polarization at pore edges becomes weaker in the ~ 5 layer GNMs compared with that of monolayer GNMs, the GNMs actually exhibited small -magnitude but evident ferromagnetism in magnetization measurements and proved presence of polarized edge spins [28].

Figure 5(a) and 5(b) show typical drain current (I_{sd}) vs. drain voltage (V_{sd}) and I_{sd} vs. back-gate voltage (V_{bg}) behaviors for a ~ 5 layer ferromagnetic GNM, respectively. In Fig.5(a), a strong zero-bias anomaly was observed. That can be attributed to either a single electron charging effect in narrow GNR regions among the nano-pores or poor interface between the Au electrodes and the GNM. Figure 5(b) displays an n-type semiconductive behavior, also due to narrow inter-pore GNR regions, which can introduce energy band gaps [17]. Because the band gaps are attributed to confinement of electrons into the one-dimensional space of the inter-pore regions (i.e., GNRs) [17], it is consistent with the presence of zigzag pore edges.

(a) Spin pumping effect under parallel fields

Figures 5(c) and 5(d) show MR (R_{xx}) behaviors for two different- W -value ferromagnetic GNMs ($W \sim 30$ nm and ~ 40 nm) for inset of Fig. 5(a)-pattern under a constant current (I_{sd}) mode of a four probe measurement, when magnetic fields are applied in parallel with the GNM planes ($B_{||}$). They show saw-tooth like MR oscillations, in which the MR monotonically increases with increasing fields, while it abruptly drops at a critical field and starts to increase

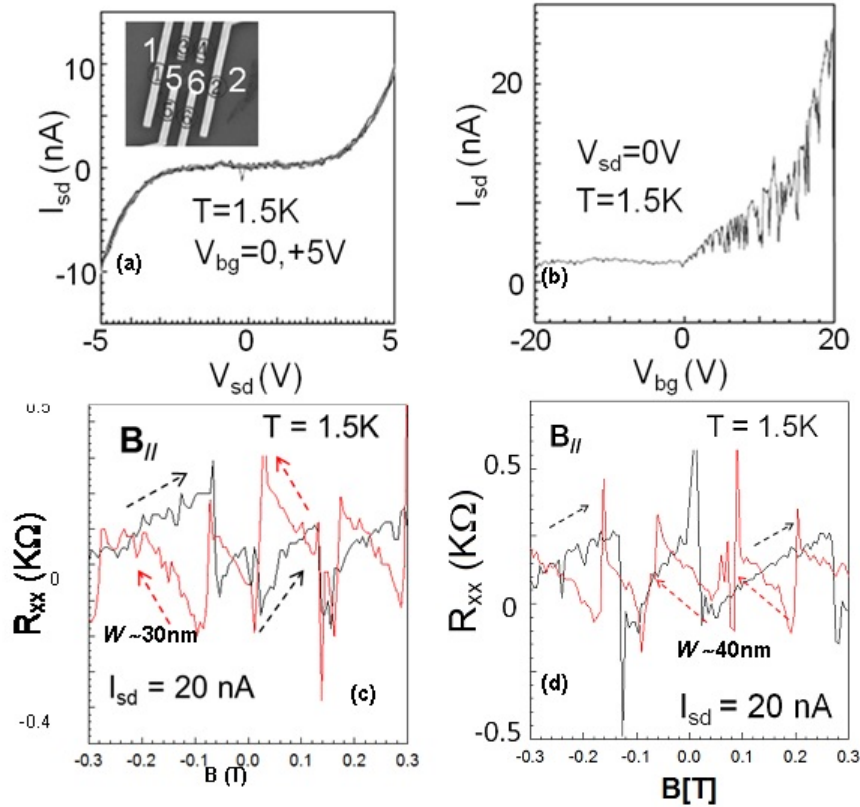


FIG. 5. (a)(b) Typical I_{sd} vs. V_{sd} (a) and I_{sd} vs. V_{bg} (b) behaviors measured between electrodes 1 and 2 (inset) in a ferromagnetic GNM with ~ 5 layers. (a) exhibits an n-type semiconductive behavior due to the narrow inter-pore regions (i.e., GNRs) (Fig. 1(e)). Inset: SEM image of Hall pattern (six probes) formed on a GNM with ~ 5 layers. MR (R_{xx}) between electrodes 5 and 6 was measured under a constant I_{sd} of 20 nA between electrodes 1 and 2. (c) (d) MR (R_{xx}) behaviors under parallel fields in different two samples with ~ 5 layers (i.e., $W \sim 30$ nm for (c) and ~ 40 nm for (d), $\phi \sim 80$ nm is common). V_{bg} was set to +20 V. Arrows mean sequence of applied B (e.g., from -0.3 T to $+0.3$ T or from $+0.3$ T to -0.3 T)

again in a repeated manner. In Fig. 5(c) for $W \sim 40$ nm, at $B < -0.05$ and $0.15 < B$, the oscillation periods are larger than those in two oscillations around $B = 0$. The periods for all oscillations are the same for increasing and decreasing B . In contrast, in Fig. 5(d) for $W \sim 40$ nm, the oscillation becomes ambiguous. We call this saw-tooth like MR oscillation as spin pumping effect. The effect means a repeated cycle of accumulation (increased number) of polarized spins and its abrupt emission (decreased number) at critical fields, depending on the applied fields. Such anomalous behaviors cannot be interpreted by any previous MR phenomena (e.g., ferromagnetic MR behavior, giant MR, tunnel MR, and spin valve effect).

In the present case, spin-polarized electrons localize at the pore edges under thermal equilibrium. However, under non-thermal equilibrium, caused by a constant current flow for Fig. 5(b), the flat bands at the pore edges are modulated and, thus, some of polarized edge-electron-spins don't localize at the pore edges and can flow through bulk graphene regions amongst the pores. In our previous ~ 10 -layer GNMs with $W \sim 20$ nm [33], the spin pumping effect was not observed under parallel fields, although MR oscillation arising from pore-edge localized electrons was found under perpendicular fields. This implies that enough inter-pore space W for electron transport between electrodes is indispensable for the spin flow and detection of the spin pumping effect (Fig. 6).

One of the qualitatively possible interpretations for the spin pumping effect might be as follows. When the applied magnetic field increases, the number of accumulated polarized-spins increase at the pore edges. Moreover, other electrons, which are flowing in bulk graphene regions among the pores, also accumulate at the flat energy band of the pore edges. However, the accumulation of edge-polarized-spins saturate and the excess spins are abruptly emitted at a critical field, as parallel magnetic fields increase further, because the flat band is modulated in the GNM plane by increasing parallel fields, more or less. After the emission of the accumulated excess spins, the flat band partially recovers to near the initial condition and the pore edges can allow further accumulation of spins. Then, MR starts to increase again. In Fig. 5(d) with $W \sim 40$ nm, the oscillation becomes ambiguous as mentioned above. This is qualitatively consistent with decrease in the ferromagnetism amplitude shown in Fig. 3(c), that is, reduction of amplitude of polarized spins at the pore edges in monolayer GNMs. This suggests the presence of optimized W values (e.g., 30 nm), which are most suitable for the appearance of a spin pumping effect. Large W values weaken the magnitude of polarized spins at the pore edges, while small W values obstruct spin flow between electrodes and make spin flow detection difficult (Fig. 6). Further clarification of the exact mechanism is expected in near future.

(b) Hysteresis loop in MR under perpendicular fields

More importantly, we confirm presence of a ferromagnetic-like MR hysteresis loop (Fig. 7), when a magnetic field is applied perpendicularly to the ferromagnetic GNM plane with $W \sim 30$ nm. Although the loop is not perfectly evident, it is somewhat reproducible. This observation can also be understood from polarized-spin transverse between electrodes due to the presence of enough interpore space as mentioned above (Fig. 6). This result is extremely important and is useful to realize all-carbon spintronic devices like magnetic semiconductors (e.g., (In, Mn), As). Indeed, this loop disappears when V_{bg} is set to -20 V in Fig. 5(b). Thus, one can control the switching of the MR hysteresis loop by changing V_{bg} . This makes feasible spin memory devices despite the absence of magnetic atoms. Magnetic semiconductors cannot work at room temperature, while the present feature in ferromagnetic GNMs appears even at room temperature (Fig. 2(d)). It, therefore, must open a new door to magnetic-atom free spintronics to resolve present environmental and resource problems.

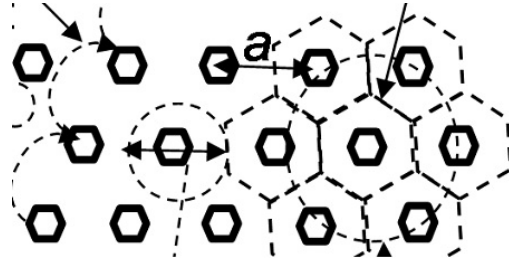


FIG. 6. Schematic top view of a GNM with current path. Under enough large W (i.g., > 30 nm), electrons including pore-edge localized spins can transvers between electrodes because of the reduced pore scattering. Cyclotron-motion electrons also form a runaway orbit and transvers, when the diameter of the motion agrees with the unit cell diameter, a

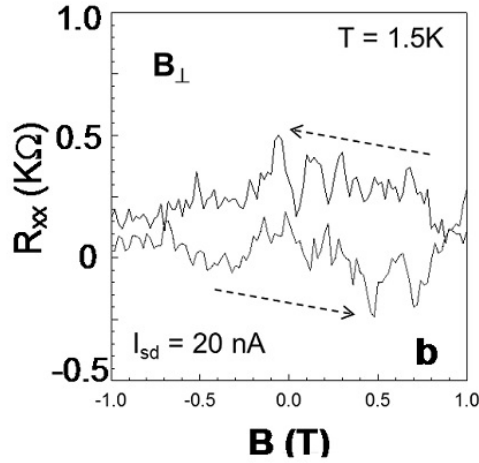


FIG. 7. MR (R_{xx}) behaviors under perpendicular fields in the sample for Fig. 5(c) with $W \sim 30$ nm. V_{bg} was also set to $+20$ V. Arrows mean sequence of applied B

3. Conclusion

In conclusion, we have successfully fabricated low-defect mono-layer GNMs by using a non-lithographic method (i.e., using NPATs as etching masks) and found the emergence of large-amplitude ferromagnetism even at room temperature, only when pore edges of the GNMs were H-terminated. The observed correlation between the inter-pore spacing and magnetism and also MFM observation supported that this was attributed to polarized electron spins localized at the zigzag pore-edges. The magnetic moment per edge dangling bond ($\sim 0.3\mu_B$) was also quantitatively in good agreement with theories for pure zigzag-GNR and also defected-GNR models (Lieb's theorem). Moreover, a spin pumping effect was found for fields applied in parallel to the GNM planes in few-layer ferromagnetic GNMs, while the MR hysteresis loop was observed under perpendicular fields. The optimized inter-pore spacing was found to be useful for detection of evident spin pumping effect and the MR hysteresis loop as well.

As mentioned in introduction, spin-based phenomena in graphenes, which were once only predicted by theories [22,25–27], have now been observed experimentally. One experiment reported on the observation of a large spin diffusion current due to the large spin coherence in high-quality graphene on a hexagonal boron-nitride substrate [32]. The other experiment mentioned in its introduction a report on the observation of SHE in dihydrogenated graphenes

by possibly introducing strong SOI, although some questions still remain. These suggest that spin-based phenomena in graphenes are approaching new stages and also the observations of present edge-spin phenomena open a new door towards the creation of novel spintronic devices. The present ferromagnetic GNMs must also be rare-element free, invisible and flexible in order to be utilized in ultra-light (wearable) magnets and spintronic devices, which can circumvent environmental and material-resource problems.

Acknowledgement

The authors thank K. Fujita, Y. Hashimoto, E. Endo, Y. Iye, S. Katsumoto, M. Yamamoto, S. Tarucha, T. Ando, T. Enoki, M. Koshino, J. Akimitsu, T. Muranaka, H. Aoki, S. Roche, P. Kim, X. Jia, and M. S. Dresselhaus for their technical contribution, fruitful discussions, and encouragement. This work at Aoyama Gakuin was partly supported by a Grant-in-aid for Scientific Research (Basic research A: 24241046) in MEXT, a High-Technology Research Center Project for private universities in MEXT, and also AFOSR grant. M.C. and H. X.Y. acknowledge support by French ANR PNANO project “Nanosim -Graphene” and Grenoble Nanosciences Foundation.

References

- [1] Nakada K., Fujita M., Dresselhaus G., Dresselhaus M. S. Edge state in graphene ribbons: Nanometer size effect and edge shape dependence. *Phys. Rev. B*, **54**, P. 17954 (1996) .
- [2] Fujita M., Wakabayashi K., Nakada K., Kusakabe K. Peculiar Localized State at Zigzag Graphite Edge. *J. Phys. Soc. Jpn.*, **65**, P. 1920 (1996).
- [3] Kusakabe K., Maruyama M. Magnetic nanographite. *Phys. Rev. B*, **67**, P. 092406(4p) (2003).
- [4] Okada S., Oshiyama A. Magnetic Ordering in Hexagonally Bonded Sheets with First-Row Element. *Phys. Rev. Lett.*, **87**, P. 146803(6p) (2001).
- [5] Lee H., Son Y.-W., et al. Magnetic ordering at the edges of graphitic fragments: Magnetic tail interactions between the edge-localized states. *Phys. Rev. B*, **72**, P. 174431 (2005).
- [6] Veiga R.G.A., Miwa R.H., Srivastava G.P. Quenching of local magnetic moment in oxygen adsorbed graphene nanoribbons. *J. Chem. Phys.*, **128**, P. 201101(3p) (2008).
- [7] Lee H., Park N., et al. Ferromagnetism at the edges of the stacked graphitic fragments: an ab initio study. *Chem. Phys. Lett.*, **398**, P. 207–201 (2004).
- [8] Asano H., Muraki S., et al. Strong magnetism observed in carbon nanoparticles produced by the laser vaporization of a carbon pellet in hydrogen-containing Ar balance gas. *J. Phys.: Cond. Mat.*, **22**, P. 334209(4p) (2010).
- [9] Enoki T., Takai K. The edge state of nanographene and the magnetism of the edge-state spins. *Sol. State Commun.*, **149**, P. 1144–1150 (2009).
- [10] Niimi Y., Matsui T., et al. Scanning tunneling microscopy and spectroscopy of the electronic local density of states of graphite surfaces near monoatomic step edges. *Phys. Rev. B*, **73**, P. 085421 (2006).
- [11] Son Y.-W., Cohen M.L., Louie S.G. Energy Gaps in Graphene Nanoribbons. *Phys. Rev. Lett.*, **97**, P. 216803(4p) (2006).
- [12] Yang L., Louie S.G., et al. Quasiparticle Energies and Band Gaps in Graphene Nanoribbons. *Phys. Rev. Lett.*, **99**, P. 186801(4p) (2007).
- [13] Shima N., Aoki H. Electronic structure of super-honeycomb systems: A peculiar realization of semimetal/semiconductor classes and ferromagnet. *Phys. Rev. Lett.*, **71**, P. 4389–4392 (1993).
- [14] Rosser J.F., Palacios J.J. Magnetism in Graphene Nanoislands. *Phys. Rev. Lett.*, **99**, P. 177204 (2007)s.
- [15] Jia X., Hofmann M., et al. Controlled Formation of Zigzag and Armchair Edges in Graphene Nanoribbons by Joule Heating. *Science*, **323**, P. 1701 (2009).
- [16] Girit C.O., Meyer J.C., et al. Graphene at the edge: Stability and Dynamics. *Science*, **323**, P. 1705 (2009).
- [17] Shimizu T., Haruyama J., et al. Large intrinsic energy bandgaps in annealed nanotube-derived graphene nanoribbons. *Nature Nanotech.*, **6**, P. 45–50 (2011).
- [18] Han M.Y., Brant J.C., Kim P. nsElectron Transport in Disordered Graphene Nanoribbons. *Phys. Rev. Lett.*, **104**, P. 056801(4p) (2010).

- [19] Wang X., Ouyang Y., et al. Room-Temperature All-Semiconducting Sub-10-nm Graphene Nanoribbon Field-Effect Transistors. *Phys. Rev. Lett.*, **100**, P. 206803(4p) (2008).
- [20] Krauss B., Nemes-Incze P., et al. Raman Scattering at Pure Graphene Zigzag Edges. *Nano Lett.*, **10**, P. 4544–4548 (2010).
- [21] Bai J., Zhong X., et al. Graphene nanomesh. *Nature Nanotech.*, **5**, P. 190–194 (2010).
- [22] Son Y.-W., Cohen M.L., Louie S.G. Half-metallic graphene nanoribbons. *Nature*, **444**, P. 347–349 (2006).
- [23] Takesue I., Haruyama J., et al. Superconductivity in Entirely End-Bonded Multiwalled Carbon Nanotubes. *Phys. Rev. Lett.*, **96**, P. 057001(4p) (2006).
- [24] Murakami S., Nagaosa N., Zhang S.-C. Dissipationless Quantum Spin Current at Room Temperature. *Science*, **301**, P. 1348–1351 (2003).
- [25] Kane C.L., Mele E.J. Quantum Spin Hall Effect in Graphen. *Phys. Rev. Lett.*, **95**, P. 226801(4p) (2005).
- [26] Kane C.L. Graphene and the Quantum Spin Hall Effect. *Int. J. Modern Phys. B*, **21**, P. 1155–1164 (2007).
- [27] Schmidt M.J., Loss D. Edge states and enhanced spin-orbit interaction at graphene/graphane interfaces. *Phys. Rev. B*, **81**, P. 165439(12p) (2010).
- [28] Otani M., Koshino M., Takagi Y., Okada S. Intrinsic magnetic moment on (0001) surfaces of rhombohedral graphite. *Phys. Rev. B*, **81**, P. 161403(R)(4p) (2010).
- [29] Yang H., Chshiev M., et al. Inducing and Optimizing Magnetism in Graphene Nanomesh. URL: <http://arxiv.org/abs/1103.4188>.
- [30] You Y.-M., Ni Z.-H., Yu T., Shen Z.X. Edge chirality determination of graphene by Raman spectroscopy. *Appl. Phys. Lett.*, **93**, P. 163112(1–3) (2008).
- [31] Soriano D., Leconte N., et al. Magnetoresistance and Magnetic Ordering Fingerprints in Hydrogenated Graphene. *Phys. Rev. Lett.*, **107**, P. 016602(4p) (2011).
- [32] Abanin D.A., Morozov S.V., et al. Giant nonlocality near the Dirac point in graphene. *Science*, **332** (6027), P. 328–330 (2011).
- [33] Shimizu T., Nakamura J., et al. Magnetoresistance oscillations arising from edge-localized electrons in low-defect graphene antidot-lattices. *Appl. Phys. Lett.*, **100**, P. 023104 (2012).